Proceedings of the 20th International Conference on Soil Mechanics and Geotechnical Engineering– Rahman and Jaksa (Eds)

Determination of stiffness parameters by means of numerical recalculation of CPTu in silty deposits

Détermination des paramètres de rigidité au moyen d'un recalcul numérique du CPTu dans les dépôts limoneux

Laurin Hauser, Simon Oberhollenzer, Helmut F. Schweiger & Roman Marte
Institute of Soil Mechanics, Foundation Engineering and Computational Geotechnics, Graz University of Technology, Austria, laurin.hauser@tugraz.at

Carla Fabris
Geoconsult ZT GmbH, Puch bei Hallein, Austria

ABSTRACT: Obtaining the required stiffness parameters for the numerical analysis of geotechnical problems is a challenging task. The present work investigates a straightforward approach where the shear modulus (G) and the modified compression and swelling indices (λ^*, κ^*) are derived based on the measured in-situ shear wave velocity and common ratios between G_0 and G as well as λ^* and κ^*. The obtained parameter set is used for the numerical recalculation of in-situ CPTu using the application G-PFE M. The proposed approach is validated by means of a parametric study where the influence of G_0/G and λ^*/κ^* is investi gated. The numerical study is based on the available data from the test site Rhesi which includes seismic flat dilatometer tests, piezocone penetration tests and laboratory tests carried out in silty deposits near Lake Constance in western Austria. Generally, the numerical recalculation of the CPTu is in good agreement with the in-situ measurements. For the considered stiffness range, a higher elastic stiffness combined with higher plastic compressibility leads to the best fit.

RÉSUMÉ: L'identification des paramètres de rigidité requis pour l'analyse numérique des problèmes géotechniques est une tâche difficile. Le présent travail étudie une approche directe où le module de cisaillement (G) et les indices de compression et de gonflement modifiés (λ^*, κ^*) sont dérivés sur la base de la vitesse des ondes de cisaillement mesurée in-situ et des rapports communs entre G_0 et G ainsi que λ^* et κ^*. Les paramètres obtenus sont utilisés pour le recalcul numérique du CPTu in-situ en utilisant l'application G-PFEM et l'influence de G_0/G et λ^*/κ^* est étudiée au moyen d'une étude paramétrique permettant d'évaluer l'approche proposée. L'étude numérique est basée sur les données disponibles du site d'essai Rhesi qui comprend des essais sismiques au dilatomètre plat, des essais de pénétration au piézocône et des essais en laboratoire réalisés dans des dépôts limoneux près du Lac de Constance dans l'ouest de l'Autriche. En général, le recalcul numérique du CPTu est en bon accord avec les mesures in-situ. Pour la gamme de rigidité considérée, des rigidités élastiques plus élevées combinées à une compressibilité plastique plus élevée conduisent à la meilleure correspondance.

KEYWORDS: cone penetration testing, silty deposits, stiffness, shear wave velocity, particle Finite Element method

1 INTRODUCTION

The determination of stiffness parameters based on in-situ investigation methods, such as piezocone penetration testing (CPTu) or flat dilatometer testing (DMT), is a crucial task in geotechnical engineering. In cone penetration testing the measured tip resistance is typically correlated to the constraint modulus M resulting in different empirical factors for different soils. Similarly, M is obtained from the intermediate DMT parameters, namely the material index I_D, the horizontal stress index K_D and the dilatometer modulus E_D, using different correlations (Schnaid, 2009). Additionally, the penetrometer can be equipped with geophones and the propagation velocity V_s of a shear wave, induced at the ground surface, is determined at different depths. Based on V_s and the bulk density of the soil the shear modulus G_0 at small strains is calculated.

Obtaining the full set of stiffness parameters for the numerical analysis of geotechnical problems, employing more advanced constitutive models, is not always straightforward due to lacking data. Therefore, certain parameters are often chosen based on experience and in relation to other known stiffnesses. In the present work, this engineering approach is investigated for silty deposits in Austria according to the following idea: Firstly, the stiffness parameters are estimated based on the measured V_s using engineering rules of thumb. The obtained set of parameters is then used for the numerical recalculation of CPTu and the results are compared to the in-situ measurements allowing for the evaluation of the approach. The available in-situ data, i.e. V_s obtained from a seismic flat dilatometer test (SDMT) and the CPTu data in terms of the corrected tip resistance q_t, sleeve friction f_s, pore pressures u_1 (mid-face position) and u_2 (shoulder position), as well as results from laboratory testing, originate from the testing campaign at test site Rhesi, as part of the research project PITS.

In the following, a brief overview of the numerical model and the in-situ testing campaign is given. Finally, the results of the numerical study are presented and discussed.

2 NUMERICAL MODEL

The simulation of cone penetration is a complex task: large displacements and deformations of the soil around the penetrometer combined with nonlinear material behaviour and the requirement to model frictional contact between the ideally rigid cone and the deformable soil result in a highly nonlinear problem. Advanced numerical methods have already been applied successfully to model cone penetration (Sheng et al., 2009; Ceccato et al., 2016; Ciantia et al., 2016; Yuan et al., 2019). In this study, the application G-PFEM (Monforte et al., 2017a, 2018), short for Geotechnical Particle Finite Element Method (PFEM), is used which has been developed within the framework Kratos (Dadvand et al., 2010).

2.1 *G-PFEM*

The PFEM solves a given boundary value problem while performing frequent remeshing of critical regions of the integration domain. At the beginning of a time step, the domain is treated as a cloud of particles/nodes that carry all information. Nodes may be added or removed based on predefined criteria, e.g., formulated in terms of a minimum element size or a threshold value for plastic strains. Then, the boundaries of the domain are defined, a new mesh is created and, eventually, the computation step is solved by means of the Finite Element Method (FEM) resulting in an updated cloud of nodes (Oñate et al., 2011). In this way, large deformations of the domain can be taken into account avoiding excessive mesh distortion. However, this comes at the cost of an increased computation time. Linear triangular elements in connection with a stabilized and mixed formulation of the quasi-static linear momentum and mass balance equations in an updated Lagrangian setting are used. The determinant of the deformation gradient, a measure for volume change, is introduced as a nodal variable in addition to the displacement vector and the water pressure (Monforte et al., 2017b). The frictional contact between cone and soil obeys a Coulomb friction law and is considered as a set of constraints on the solution enforced using a penalty method. A more detailed outline of G-PFEM is given in Monforte et al. (2017a).

The material behaviour is modelled employing the Clay and Sand Model (CASM), a state-parameter-based, elastic-plastic critical state model proposed by Yu (1998). In this model, the shape of the yield surface is controlled through the parameters r and n which makes the model adaptable to a wider range of geomaterials. Figure 1 illustrates the influence of r and n showing that the surfaces of the Original Cam Clay model (OCCM) and the Modified Cam Clay model (MCCM) may be obtained for particular combinations of r and n. The implemented version of the model incorporates the hyperelastic model by Houlsby (1985) where the modified swelling index κ^* and the shear modulus G control the volumetric and deviatoric behaviour, respectively. The parameter α allows for coupling of the volumetric and deviatoric response, however, in this work $\alpha = 0$ is assumed. According to the classical critical state hardening rule, the preconsolidation pressure is a function of the plastic volumetric strain and the compressibility parameters κ^* and λ^*, the latter being the modified compression index. The model has been adapted to finite strains according to Monforte et al. (2015).

The CASM and its extension for structured soils have already been used to investigate cone penetration in structured and brittle material using G-PFEM (Hauser and Schweiger, 2021; Monforte et al., 2021).

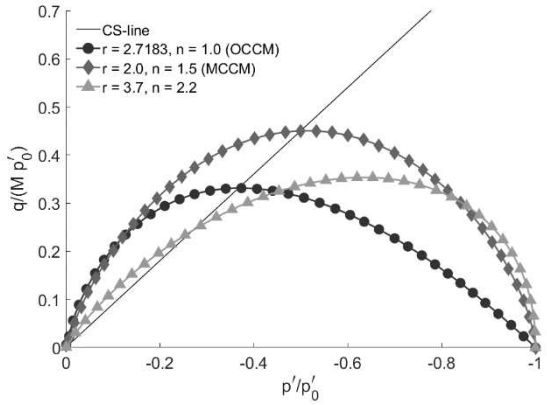

Figure 1. CASM yield surface for different combinations of r and n in the p'-q space normalized with respect to the respective preconsolidation pressure p'_0.

2.2 *CPTu model*

An axisymmetric model is used including a rectangular, deformable soil body (height of 2.2 m and width of 1.0 m) and a rigid cone with a tip angle of 60° and a radius R of 2.19 cm (equivalent to 15 cm² base area). The lateral and lower boundaries are fixed in normal direction and an overburden pressure is applied on top of the domain (see Figure 2). At the beginning of the computation, the penetrometer is already located in the soil (at a depth of 0.2 m) before the downwards movement at a velocity of 2 cm/s is initiated. Assuming weightless soil a constant initial stress field is imposed and after an initial transient phase of roughly 10 radii of penetration stationary values of q_t, f_s, u_1 and u_2 are obtained (see Figure 5). The choice of the numerical parameters, e.g. the initial mesh, the criteria for mesh refinement or the contact stiffness, are based on previous studies (Hauser and Schweiger, 2021).

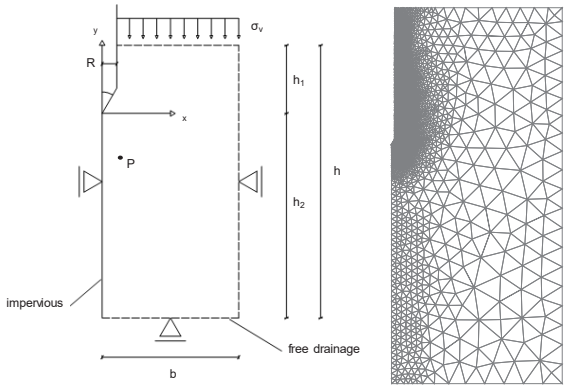

Figure 2. Axisymmetric model and refined mesh during penetration.

3 TEST SITE

The ongoing research project PITS, initiated at TU Graz in cooperation with the Federal Chamber of Architects and Chartered Engineering Consultants, focuses on an improved characterization of postglacial silty deposits in Austria. The project involves extensive in-situ testing campaigns at different test sites in Austria. Additionally, soil specimens are recovered for laboratory testing. Data obtained at test site Rhesi, located in the forelands of the river Rhine near Lake Constance in western Austria, is considered in the present work including CPTu tests carried out at the standard penetration rate of 2 cm/s using u_1 and u_2 probes as well as SDMT tests. Figure 3 shows the obtained profiles of q_t, f_s, u_1, u_2 and V_s over depth. The homogeneous layer of clayey silt (layer L3) starting at a depth of roughly 13 m below the ground surface is of main interest for the present work. The vertical permeability $k_v = 6.2*10^{-9}$ m/s and the friction angle φ = 27° were determined through laboratory testing.

4 DETERMINATION OF STIFFNESS PARAMETERS

The present study aims to evaluate the choice of stiffness parameters for silty deposits based on the measured shear wave velocity V_s. Therefore, the following approach is adopted using the available data of test site Rhesi: Firstly, the small-strain shear modulus G_0 is calculated from the measured V_s and the bulk density ρ:

$$G_0 = V_s^2 \cdot \rho \tag{1}$$

Extensive research has been conducted regarding the ratio between G_0, obtained from SDMT, and the shear modulus at larger working strains G_{DMT} (in the following equivalent to G) for different soil types. Marchetti and Monaco (2018) proposed

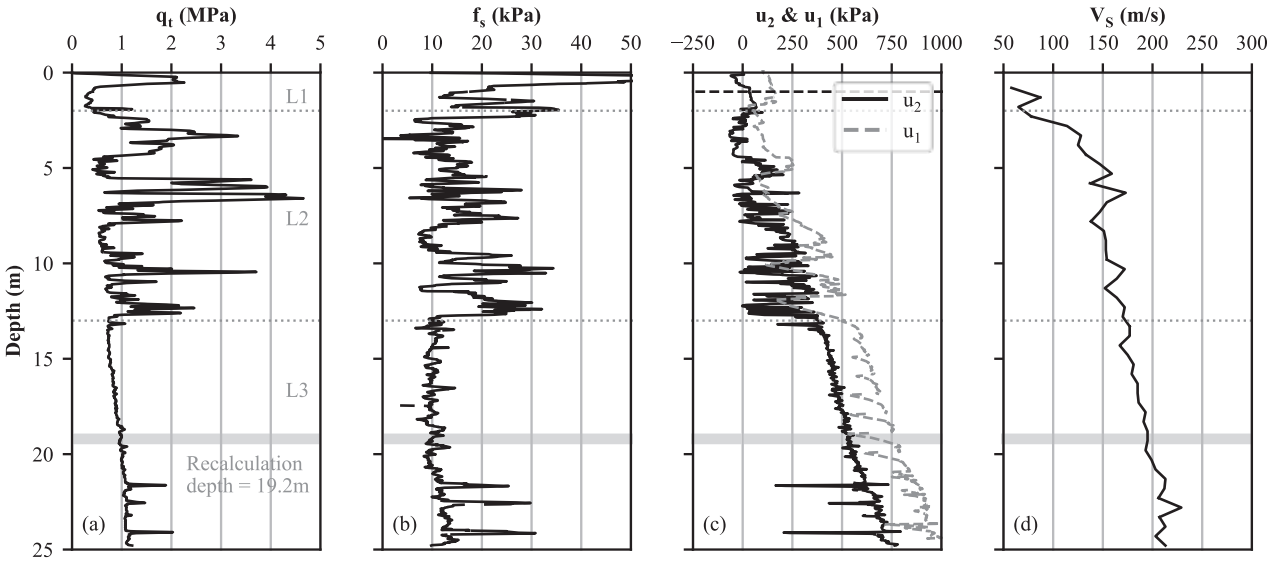

Figure 3. Overview of in-situ measurements (q_t, f_s, u_1, u_2, V_S) over depth at test site Rhesi; depth for the numerical recalculation marked at 19.2 m below the ground surface.

a value of around 4.2 for G_0/G_{DMT} which was obtained from a silty-clayey site in Italy. In the following numerical study, the ratio G_0/G is treated as a variable.

According to linear elasticity, the bulk modulus K is calculated from G assuming a Poisson's ratio $\upsilon = 0.2$. Consequently, the modified swelling index κ^* is obtained for the in-situ effective mean stress p' of 128 kPa (for $K_0 = 0.55$):

$$K = \frac{2 \cdot G \cdot (1+\nu)}{3 \cdot (1-2\nu)} \quad (2)$$

$$\kappa^* = \frac{p'}{K} \quad (3)$$

The modified compression index λ^* is defined as a multiple of κ^* through the ratio λ^*/κ^* which is varied in the following study. Thus, the numerical recalculation of the in-situ CPTu is carried out for different sets of G, κ^* and λ^* which are based on V_s, G_0/G and λ^*/κ^*. The results are compared to the actual test data allowing for the evaluation of the proposed approach. The CASM does not account for effects of small-strain stiffness which are expected to be of minor importance given the large strains occurring during cone penetration.

5 NUMERICAL RECALCULATION OF CPTU

The basic parameter set for the recalculation of the in-situ CPTu is summarized in Table 1. Due to the lack of more specific data e.g. from triaxial testing, the CASM parameters r and n are defined in such a way that the elliptical yield surface of the Modified Cam Clay model is obtained. Weightless soil is assumed resulting in a constant initial stress field with σ'_v = 183 kPa, σ'_h = 100 kPa and u_0 = 179 kPa. This corresponds to the in-situ depth of 19.2 m. The overconsolidation ratio (OCR) is equal to 1 and no coupling between volumetric and deviatoric behaviour is considered ($\alpha = 0$). The friction angle and the vertical permeability were directly obtained from laboratory testing.

To evaluate the choice of stiffness parameters based on V_s different ratios for G_0/G (equal to 4, 5, 6) and λ^*/κ^* (equal to 3, 6, 9) are used for a parametric study covering realistic ranges (Wang et al., 2017; Marchetti and Monaco, 2018). The resulting input parameters are outlined in Table 2.

Table 1. Material parameters for the numerical recalculation of test site Rhesi.

γ [kN/m³]	**φ [°]**	**k_v [m/s]**	**OCR [-]**
0	27	$6.2*10^{-9}$	1
r [-]	**n [-]**	**α [-]**	**K_0 [-]**
2	1.5	0	0.55

Table 2. Stiffnesses G, κ^* and λ^* for the parametric study on G_0/G and λ^*/κ^*.

G_0/G		**4**	**5**	**6**
G [kPa]		17800	14200	11900
κ^* [-]		0.0054	0.0067	0.0081
	λ^*/κ^*			
λ^* [-]	**3**	0.0162	0.0201	0.0243
	6	0.0324	0.0402	0.0486
	9	0.0486	0.0603	0.0729

Initially, an interface friction angle $\varphi_{int} = \varphi/3 = 9°$ was chosen for the present study. The resulting friction coefficient $\tan(\varphi_{int})$ is slightly below the proposed range of 0.2 to 0.35 for low plasticity clays according to Lemos and Vaughan (2000). The influence of φ_{int} was evaluated during the numerical study.

The horizontal permeability k_h has a significant influence on the (predominantly radial) dissipation of the generated pore pressure around the penetrometer. Therefore, the dissipation curves obtained from the numerical simulation have been compared to the in-situ results assuming both isotropic ($k_h = k_v$) and anisotropic permeability ($k_h = 10*k_v$). Figure 4 shows that an increased horizontal permeability reduces the dissipation time significantly compared to the isotropic case which agrees well with the in-situ dissipation curves. Thus, isotropic permeability was assumed for the recalculation.

Figure 6 compares the in-situ measurements, obtained from two different tests with the piezometer located at the u_1 or u_2 position respectively, and the results of the numerical recalculations for different stiffness ratios (G_0/G, λ^*/κ^*) and interface friction angles (6°, 9°, 12°) in terms of tip resistance q_t over sleeve friction f_s and pore pressure u_1 and u_2 at the

considered depth of 19.2 m. Two exemplary profiles of the recalculated q_t, f_s, u_1, u_2, u_3 are presented in Figure 5.

Overall, the numerical results show the same order of magnitude compared to the in-situ measurements. An increased ratio of G_0/G leads to lower tip resistance, lower pore pressure u_1 and higher sleeve friction, independently of φ_{int}. A reduction of the ratio λ^*/κ^* leads to an increase of q_t, f_s and u_1, again independently of φ_{int}. The pore pressure u_2 appears to be slightly affected by G_0/G and almost unaffected by λ^*/κ^*. Generally, an increase of φ_{int} leads to higher q_t and f_s while u_1 and u_2 appear to be less influenced by φ_{int}.

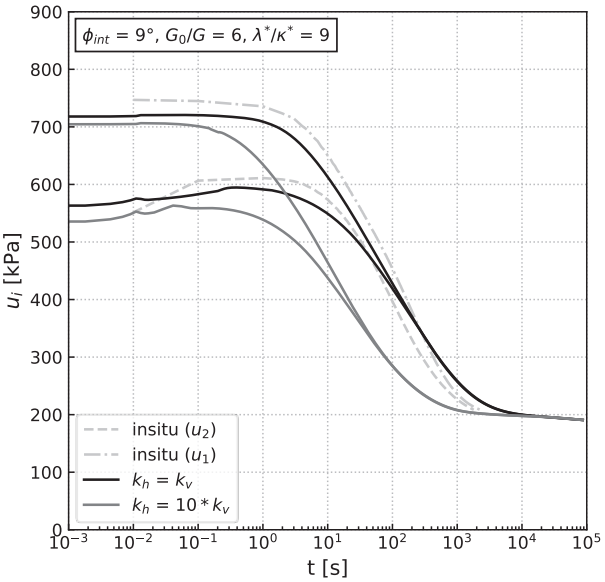

Figure 4. Comparison of the in-situ and numerical pore pressure dissipation curves at positions u_1 and u_2 considering isotropic ($k_h = k_v$) and anisotropic permeability ($k_h = 10*k_v$).

6 DISCUSSION

The ratio G_0/G governs the elastic stiffness parameters. A large value of G_0/G leads to a reduction of G and an increase of κ^* since G_0 is constant. As q_t and u_1 decrease with reduced elastic stiffnesses the effective mean stress around the cone increases. This leads to an increase of the effective horizontal stresses and, consequently, to higher sleeve friction (compare Figure 6). The observed increase of f_s reaches up to 5 kPa for the highest considered φ_{int} of 12° and is expected to be of minor practical relevance, however, the observation is consistent with the used hyperelastic model where the Poisson's ratio increases with the effective mean stress. A larger ratio λ^*/κ^* implies a higher plastic compressibility λ^* (for a fixed value of κ^*) leading to lower values of q_t, f_s and u_1.

Good agreement between the in-situ and the recalculated tip resistance, i.e. the numerical q_t lies within the two in-situ results obtained with the u_1 and the u_2 probe, is found either for lower elastic stiffnesses (high value of G_0/G) combined with lower plastic compressibility (low value of λ^*/κ^*) or, vice versa, for higher elastic stiffnesses combined with high plastic compressibility. The same observation is valid for the comparison of the measured and calculated u_1 pore pressure which varies up to 10%, around 80 kPa, for the considered stiffness ratios G_0/G and λ^*/κ^*. The comparison suggests that a lower value of G_0/G leads to a better agreement between the in-situ measurement and the numerical result for u_1. The pore pressure u_2 is not noticeably affected by a change of λ^* and increases slightly for higher elastic stiffnesses. For the considered range of φ_{int}, the calculated and the in-situ sleeve friction match when higher elastic stiffnesses combined with high plastic compressibility are used. In this context, the assumption $\varphi_{int} = \varphi/3 = 9°$ leads to reasonable results considering that φ_{int} of 6° is well below the values suggested in the literature and an increased φ_{int} of 12° leads to a significant increase of f_s compared to the in-situ measurements, however, some uncertainty associated with the choice of φ_{int} remains.

All in all, the results show that the recalculation of the in-situ CPTu reproduces consistent results compared to the measurements. The best agreement, though, is found for rather high elastic stiffnesses (lower values of G_0/G) combined with high plastic compressibility (higher value of λ^*/κ^*).

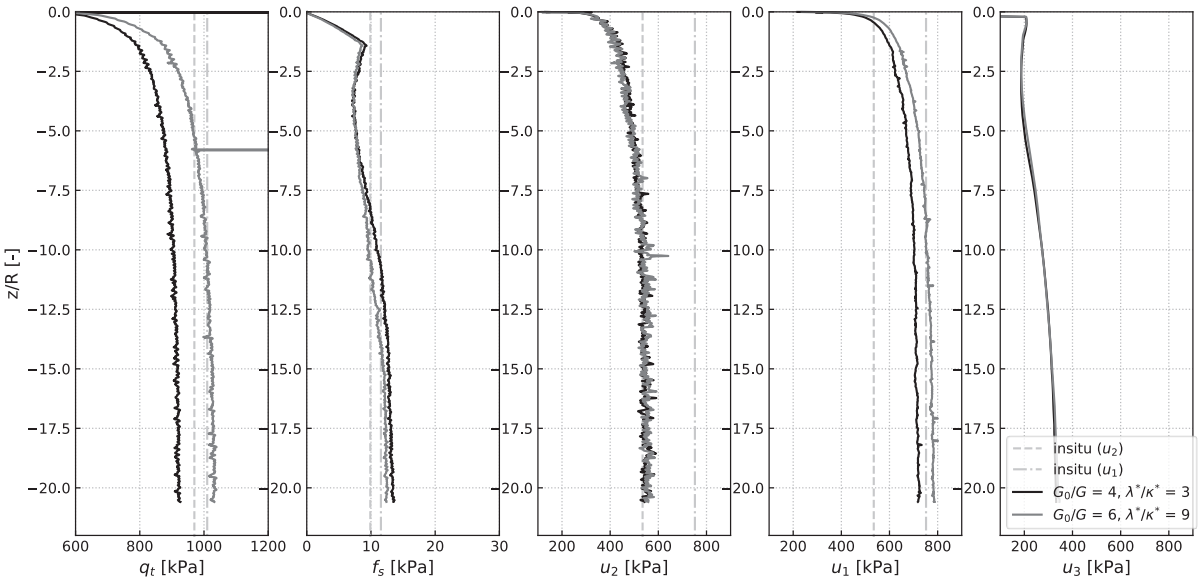

Figure 5. Results of the numerical recalculation in terms of q_t, f_s, u_1, u_2, u_3 over normalized depth for a constant initial stress field, representing the in-situ depth of 19.2 m below the ground surface, compared to the results of the two in-situ tests using the u_1 and u_2 piezocone, respectively.

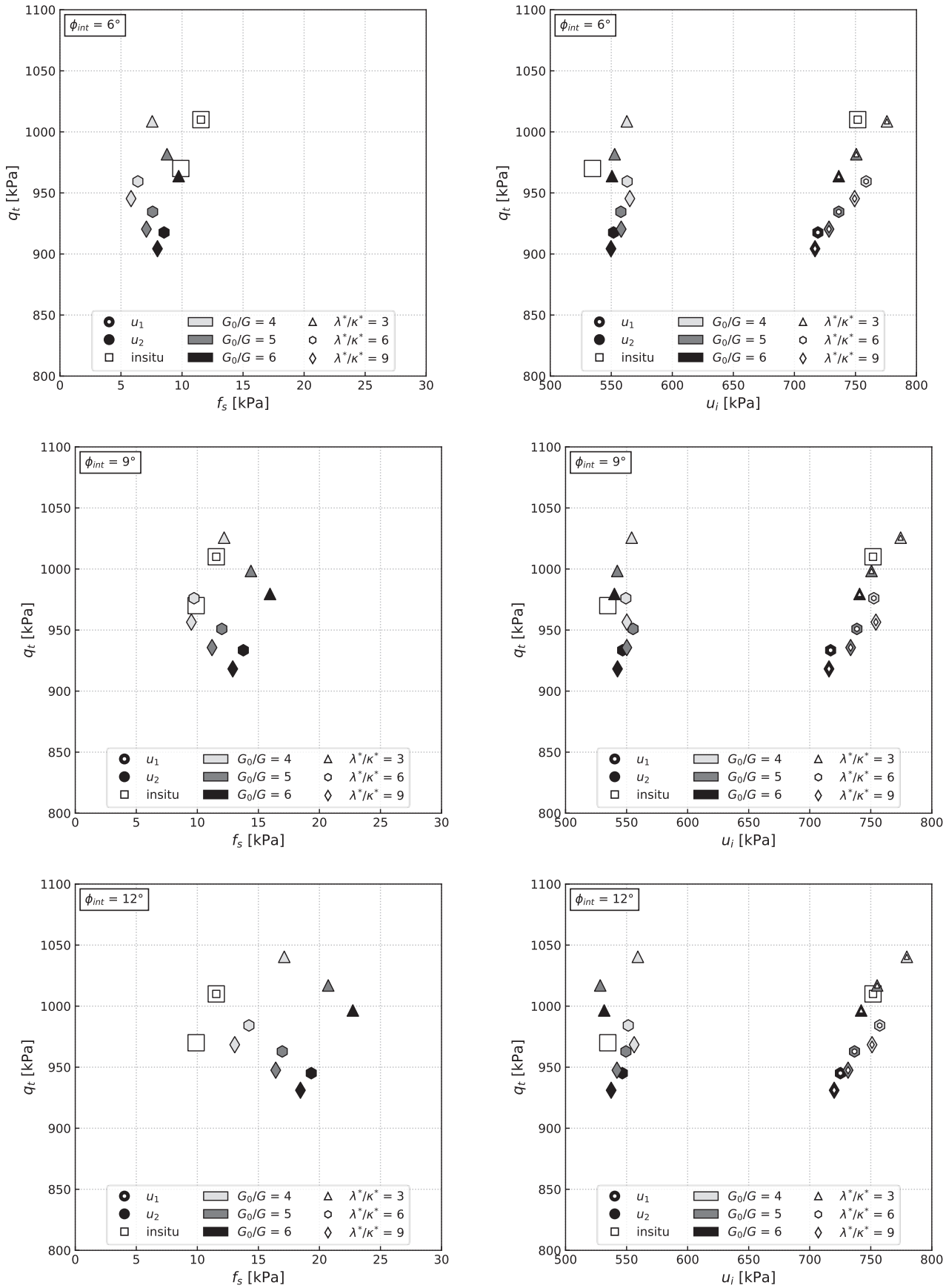

Figure 6. Comparison of in-situ measurements (square white markers) and numerical recalculations for different stiffness ratios (G_0/G, λ^*/κ^*) and interface friction angles (6°, 9°, 12°) in terms of tip resistance q_t over sleeve friction f_s and pore pressure u_1 and u_2 at the depth of 19.2 m; empty symbols represent results at the u_1 position (obtained from the numerical calculation or measured in-situ) and full symbols at the u_2 position.

7 CONCLUSION

The presented numerical study shows that in-situ CPTu can be successfully recalculated using the application G-PFEM. The stiffness parameters, i.e. G, κ^* and λ^*, have been derived from the measured shear wave velocity V_s in a straightforward approach using common relations between G_0 and G as well as κ^* and λ^*. Combining higher elastic stiffnesses (G, κ^*) and higher plastic compressibility (λ^*) leads to the best agreement with the in-situ measurements for the considered silty deposits.

8 ACKNOWLEDGEMENTS

The authors acknowledge the financial and logistical support provided by the Austrian Research Promotion Agency and the Federal Chamber of Architects and Chartered Engineering Consultants.

9 REFERENCES

Ceccato F., Beuth L., Vermeer P.A. and Simonini P. 2016. Two-phase Material Point Method applied to the study of cone penetration. *Computers and Geotechnics* 80, 440–452.

Ciantia M.O., Arroyo M., Butlanska J. and Gens A. 2016. DEM modelling of cone penetration tests in a double-porosity crushable granular material. *Computers and Geotechnics* 73, 109–127.

Dadvand P., Rossi R. and Oñate E. 2010. An Object-oriented Environment for Developing Finite Element Codes for Multi-disciplinary Applications. *Archives of Computational Methods in Engineering* 17(3), 253–297.

Hauser L. and Schweiger H.F. 2021. Numerical study on undrained cone penetration in structured soil using G-PFEM. *Computers and Geotechnics* 133.

Houlsby G.T. 1985. The use of a variable shear modulus in elastic-plastic models for clays. *Computers and Geotechnics* 1(1), 3–13.

Lemos L.J.L. and Vaughan P.R. 2000. Clay–interface shear resistance. *Géotechnique* 50(1).

Marchetti S. and Monaco P. 2018. Recent Improvements in the Use, Interpretation, and Applications of DMT and SDMT in Practice. *Geotechnical Testing Journal* 41(5).

Monforte L., Arroyo M., Carbonell J.M. and Gens A. 2017a. Numerical simulation of undrained insertion problems in geotechnical engineering with the Particle Finite Element Method (PFEM). *Computers and Geotechnics* 82, 144–156.

Monforte L., Arroyo M., Carbonell J.M. and Gens A. 2018. Coupled effective stress analysis of insertion problems in geotechnics with the Particle Finite Element Method. *Computers and Geotechnics* 101, 114–129.

Monforte L., Arroyo M., Gens A. and Carbonell J.M. 2015. Integration of elasto-plastic constitutive models in finite deformation: An explicit approach. *In Computational Plasticity XIII Fundamentals and Application: Proceedings of the XIII International Conference on Computational Plasticity* (Oñate E, Owen DRJ, Peric D and Chiumenti M (eds)). International Center for Numerical Methods in Engineering (CIMNE), Barcelona, Spain, 398–406.

Monforte L., Carbonell J.M., Arroyo M. and Gens A. 2017b. Performance of mixed formulations for the particle finite element method in soil mechanics problems. *Computational Particle Mechanics* 4(3), 269–284.

Monforte L., Gens A., Arroyo M., Mánica M. and Carbonell J.M. 2021. Analysis of cone penetration in brittle liquefiable soils. *Computers and Geotechnics* 134.

Oñate E., Idelsohn S.R., Celigueta M.A. et al. 2011. Advances in the Particle Finite Element Method (PFEM) for Solving Coupled Problems in Engineering. I*n Particle-based methods: Fundamentals and applications* (Oñate E and Owen DRJ (eds)). Springer, Dordrecht, London, vol. v. 25, 1–49.

Schnaid F. 2009. In situ testing in geomechanics: The main tests / Fernando Schnaid. Taylor & Francis, London.

Sheng D., Nazem M. and Carter J.P. 2009. Some computational aspects for solving deep penetration problems in geomechanics. *Computational Mechanics* 44(4): 549–561.

Wang W.D., Li Q. and Xu Z.H. 2017. Determination of parameters for hardening soil small strain model of Shanghai clay and its application in deep excavations. *In Proceedings of the 19th International Conference on Soil Mechanics and Geotechnical Engineering* (Lee W (ed.)). Korea Geotechnical Society, 2065–2068.

Yu H.S. 1998. CASM: a unified state parameter model for clay and sand. *Int. J. Numer. Anal. Meth. Geomech.* 22, 621–653.

Yuan W.-H., Zhang W., Dai B. and Wang Y. 2019. Application of the particle finite element method for large deformation consolidation analysis. *Engineering Computations* 36(9).